

Electron interferometry with nano-gratings

Alexander D. Cronin and Ben McMorran

Department of Physics, University of Arizona, Tucson, AZ 85721

(Dated: May 6, 2019)

We present an electron interferometer based on near-field diffraction from two nanostructure gratings. Lau fringes are observed with an imaging detector, and revivals in the fringe visibility occur as the separation between gratings is increased from 0 to 3 mm. This verifies that electron beams diffracted by nanostructures remain coherent after propagating farther than the Talbot length $z_T = 2d^2/\lambda = 1.2$ mm, and hence is a proof of principle for the function of a Talbot-Lau interferometer for electrons. Distorted fringes due to a phase object demonstrates an application for this new type of electron interferometer.

Near-field interference effects that result in self-similar images of a periodic structure were noticed by Talbot in 1836, and later described as Fourier images [1, 2, 3]. One remarkable feature is that revivals in image visibility occur periodically as the plane of observation is separated from the periodic structure. The visibility of self-images is maximized at half-integer multiples of the Talbot distance $z_T = 2d^2/\lambda$, with d being the period of the structure and λ the wavelength of the light or de Broglie waves illuminating the structure. Partially coherent waves are required to observe self-images of a single grating (the Talbot effect). However, a related phenomenon (the Lau effect) occurs with incoherent light if *two* gratings are used [3, 4, 5]. Fringes are then formed behind the second grating, and the fringe visibility oscillates as a function of grating separation. These Lau fringes have maximum visibility on a distant screen when the gratings are separated by nd^2/λ , with n being an integer. In a Talbot-Lau interferometer, Lau fringes are detected with the aid of a third grating, but the fringes can also be observed directly on a screen, thus making a Lau interferometer as shown in Figure 1.

Here we present a Lau interferometer for electrons based on two nanostructure gratings that each have a period of $d = 100$ nm. With medium energy (5 keV) electrons that have a de Broglie wavelength of $\lambda = 17$ pm, the Talbot length is 1.16 mm. An imaging detector 80 cm beyond the gratings was used to observe the Lau fringes shown in Figure 2, and the fringe visibility as a function of grating separation is plotted in Figure 3. If the fringes are analyzed with a third grating (even a digital grating in the image processing can achieve this purpose), then this apparatus serves as a Talbot-Lau interferometer. However, even more information is gained by studying images of the Lau fringes directly.

Interferometers based on the Talbot and Lau effects have found applications in light optics [3, 5, 6], in atom optics [7, 8, 9, 10, 11], and more recently with x-rays [12]. Yet even though electron interferometry is a mature field [13, 14, 15], neither Lau nor Talbot-Lau interferometer designs have been operated with electrons until now.

Perhaps the chief reason that Talbot-Lau interferometers have not previously been created for electrons is that suitable periodic structures have not been available. Crystals with a lattice period on the order of 1 nm can

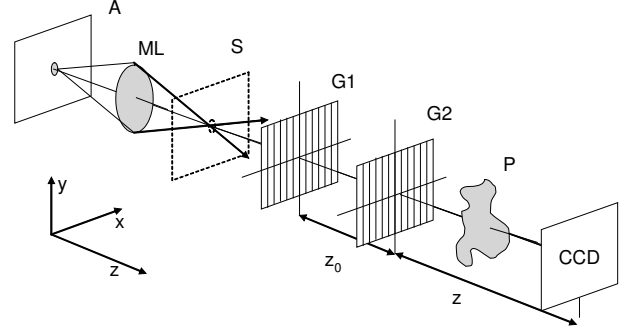


FIG. 1: Lau interferometer for electrons. A, 100- μ m aperture; ML, magnetic lens; S, the electron beam converges to a 10 μ m spot in this plane; G1, nano-grating; G2, 2nd nano-grating; P, phase object; CCD, imaging screen. In our experiments z_0 is in the range 0-3 mm, and $z=80$ cm. The distance between S and G1 is typically 2 cm, and the divergence of the beam from S is 5×10^{-3} radians. Not shown: the thermionic tungsten filament, grid cap, and condenser lens are located before A.

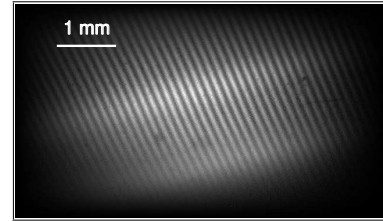


FIG. 2: Lau fringes formed with 5 keV electrons and two 100-nm period gratings separated by 0.6 mm (half the Talbot length). This figure was obtained by imaging a phosphor screen with a CCD.

serve as a grating, but the resulting Talbot length of 200 nm is too short for many practical interferometer experiments [16]. A further complication is that the angular misalignment of the two gratings must be smaller than one grating period over the height of the beam. Hence alignment within 10^{-6} radians is required when using crystal gratings and a 1 mm high beam. These limitations are overcome by using nanostructure gratings with a 100 nm period. Then the talbot length is increased to 1 mm, and the alignment tolerance is relaxed to 10^{-3} radians.

Nanostructures for electron optics are new. The gratings that we use are fabricated at MIT [17], and were only recently used to study electron diffraction [18, 19]. Similar gratings have enabled several atom interferometers [9, 10, 20, 21], and thicker gratings have given first light to x-ray Talbot interferometers [12]. That nanostructures can be used for coherent electron optics was not obvious for several reasons. Local charging of the nano-structures, non-uniform image charge interactions with the nano-structures, and the possibility of coulomb drag and electron energy loss due to passing within a few nanometers of a surface are just a few mechanisms that could lead to decoherence. Our results show that sufficient coherence is maintained to operate an electron interferometer with nanostructure gratings.

In the rest of this paper we describe the electron optics setup, and the diffraction theory used to study the revivals in Figure 3. We comment on the role of image charge interactions between electrons and the nano-gratings. Then we demonstrate an application of this interferometer: the study of the index of refraction for electrons due fields around a charged needle tip.

The Lau fringes have highest visibility when the grating separation (z_0) and the distance to the screen (z) satisfy

$$\frac{z_0 z}{z_0 + z} = \frac{nd^2}{\lambda}. \quad (1)$$

Then the period of the Lau fringes is

$$d' = d \frac{z_0 + z}{z_0}. \quad (2)$$

where d is the period of the gratings. Equations 1 and 2 are derived in the Fresnel approximation in references [3, 6, 11]. Because the distance to the screen is typically 800 times as long as the separation between gratings ($z/z_0 = 800$) in our experiment, the fringes are effectively magnified so that $d' = 800d$. The ratio of periods for G1, G2 and the detected fringes is therefore 1:1:800.

To describe in detail the shape and visibility, $V \equiv (max - min)/(max + min)$, of the fringes as a function of grating separation we relied on a calculation given in Equation 3 of reference [11]. Briefly, the concept is that the first grating is considered to be a set of mutually incoherent point sources of monochromatic waves. Waves from each point source are diffracted by G2 and arrive at the imaging screen in the near-field (Fresnel) diffraction regime. The intensity pattern on the screen is generated by adding diffraction patterns from each point source. Grating G1 and the screen define the position of many sources and detectors; they function as classical components. In contrast, grating G2 acts as a quantum mechanical diffraction object. This theory was used to generate the curves in Figure 3 and the theoretical portion of Figure 4.

We are justified in considering incoherent illumination of G1 by the van Cittert-Zernike theorem, which gives

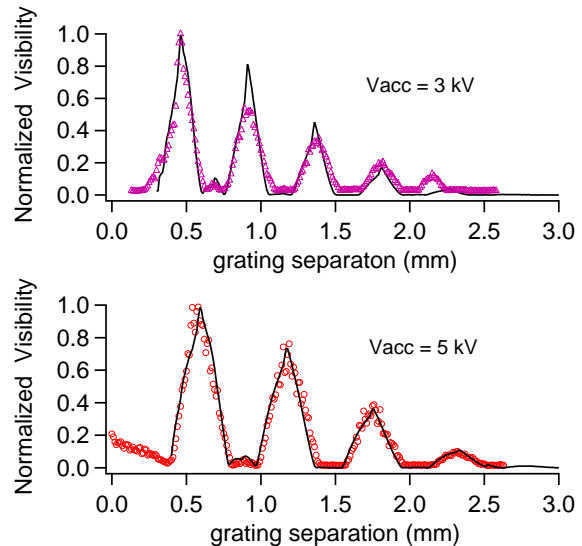


FIG. 3: Revivals in fringe visibility as a function of grating separation (z_0). Data (symbols) are compared to theory (line) from reference [11] for two gratings each with 35% open fraction. Visibility maxima are found when the gratings are separated by a half integer number of Talbot lengths, and this depends on the electron accelerating voltage (V_{acc}). The maximum visibility is 30% for both the 3keV and 5keV electrons. Visibility decays when the fringe period is comparable to the resolution of the detector.

the transverse coherence length, $\ell_{tcoh} \approx \lambda/\theta$ in terms of θ , the angle subtended by the source. The electron beam is focused to a $10 \mu\text{m}$ spot just 2 cm in front of G1 (see figure 1) and the spot size in this plane cannot be made smaller because of the extended electron source and lens aberrations. This corresponds to a coherence length of $\ell_{tcoh} = 10 \text{ nm}$, which is smaller than the grating period of $d = 100 \text{ nm}$.

As remarked in reference [11], the essential coherent effect is diffraction at the second grating. The first grating simply serves as an array of sources, and the fringes could be detected by a transmission mask (with a period d') and an integrating detector. One virtue of using an imaging detector, with a digital sampling density of 100 pixels per mm, is that we can study fringes of varying period (d') as the grating separation (z_0) is changed. Images also reveal the *fractional Talbot effect* by showing fringes of half the period compared to that given by Equation 2, when the grating separation is three quarters of the Talbot length, $z_0 = 3/4 z_T$. The fractional Talbot effect was also observed with $z_0 = 1/4 z_T$.

Our experimental data are best fit by a grating transmission function for G1 and G2 that is described by a 35% open fraction, and a weak image-charge interaction between electrons and the grating bars. Image-charge interactions were discussed in detail in [18, 19], and they have a similar effect on the electron optics as the Casimir-Polder interaction does for atom optics [11, 22, 23]. We include the strength of the image-charge and the phys-

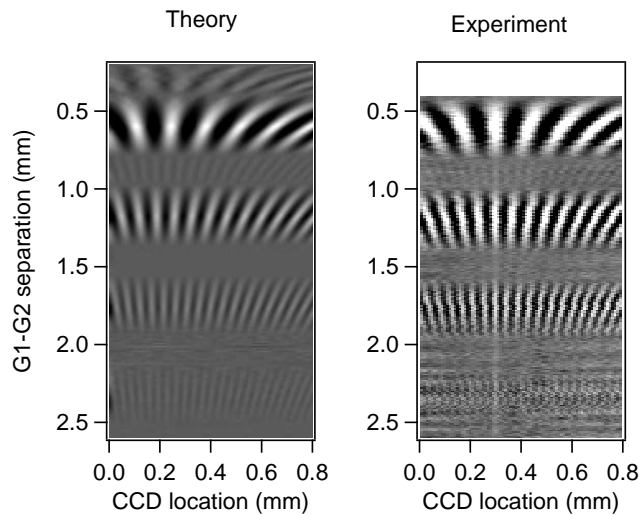


FIG. 4: Lau fringes vs. grating separation. Each row in this composite image represents a row from a different raw image. The raw images were taken with different values of G1-G2 separation (z_0). The theoretical composite was generated with the theory given in reference [11]. A point spread function for the imaging detector (Gaussian with rms = 40 μ m), and the open fraction of the gratings (35%) is included in the theory.

ical size of the grating windows as two free parameters in the transmission function for the second grating. The best fit image charge for 3 keV electrons is $q' = 0.03|e|$, and the best fit image charge for 5 keV electrons is only $q' = 0.01|e|$. This suggests that the electron-surface interaction at the nanometer scale depends on the velocity of electrons with respect to the surface. More research to investigate this is under way.

Additional analysis of the shape of the fringes was accomplished by taking the Fourier transform of images such as Figure 2. These image transforms show how the spatial frequency of the fringes change with grating separation. A composite image of fringe spectra, in which each column represents the spatial frequency spectrum of fringes for a specific grating separation (z_0), is shown in Figure 5. The fractional Talbot effect is clear at the grating separation $z_0 = 0.85$ mm. The higher harmonics of spatial frequency indicate that the fringes are not purely sinusoidal, but tend in places to look more like the binary (Ronchi rule) masks made by ideal absorbing nanostructure gratings. This is the self-imaging property of the Talbot and Lau effects.

To demonstrate that this interferometer can be used to study phase shifts for electrons due to various objects, we inserted a charged wire in the beam after the second grating in plane P of Figure 1. Like a lightning rod, the tip of the wire causes large gradients in electric potential. The electric potential in the space around the wire changes the index of refraction for electron waves and distorts the interference fringes as shown in Figure 6.

Multiple paths through the interferometer sample different parts of the phase object, therefore we are

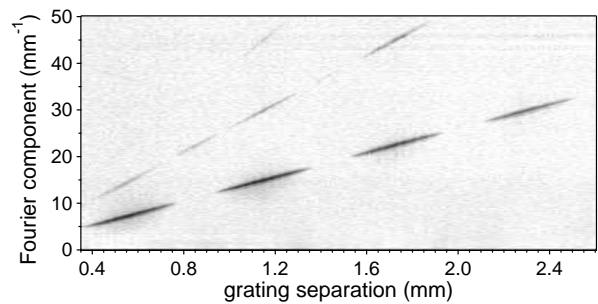


FIG. 5: Power spectra of Lau fringes vs. grating separation. Each column is given by the Fourier transform of a different row of data in Figure 4.

sensitive only to gradients in phase, not phase directly. This design is known as a shearing interferometer and shifts in fringe position are proportional to $[\partial/\partial x]\Phi(x, y)$ and distortion in the fringes is associated with $[\partial/\partial x]^2\Phi(x, y)$, where $\Phi(x, y) = \int n(x, y, z)k_0 dz$, with $n(x, y, z)$ being the index of refraction [3, 5, 6, 12, 13, 14, 15]. For electron de Broglie waves this is $\Phi(x, y) = \int \sqrt{(2m/\hbar^2)[E + |e|V(x, y, z)]} dz$ where $V(x, y, z)$ is the electric potential, E is the incident energy of the electrons, m the electron mass, e the magnitude of the electron charge, and \hbar is Planck's constant divided by 2π .

Because phase gradients are caused by energy gradients, i.e. forces, the sensitivity demonstrated here is not different in principle from a deflection sensor that can study classical forces on electrons. However, the virtue of the interferometer is still apparent because the fringes make it easier to detect deflections. One advantage is that the fringe period is 10 times finer than the smallest focus that could be produced with the incoherent beam and aberrations of the lens system in this apparatus. Second, the fringes are formed simultaneously over a large spatial region without scanning the beam.

A continuous wire produces a uniform linear phase gradient ($\nabla\Phi(x, y)$) with opposite sign on either side of the wire. That is how it serves as a bi-prism [15]. Around the tip of the freely suspended charged wire, however, there is a strong double gradient term ($\nabla^2\Phi(x, y)$). Hence fringe distortion is expected around the tip of the charged wire, and uniform fringe shifts are expected along the sides of the charged wire. Since the shifts are perpendicular to the wire, and in general the wire can be skew to the grating bars, fringes on either side of the wire can appear out of step as indicated in figure 6. This serves as a proof of principle that the interferometer setup presented here can be used to study differential phase shifts due to a phase object.

At the time of writing of this manuscript, we are aware of the construction of a Mach-Zehnder electron interferometer in the group of H. Batelaan, which requires a much higher degree of electron spatial coherence than our interferometer. Our results are distinct in that we use an incoherent electron beam and we image electron interfer-

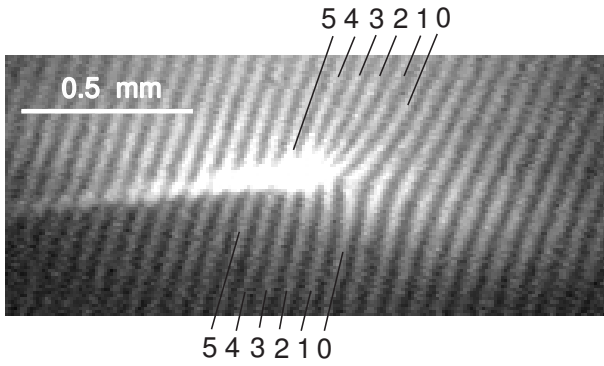


FIG. 6: Distorted fringes around the shadow of a charged wire. Consecutive fringes are labelled on the top and bottom to emphasize the discontinuity that arises due to the wire acting as a bi-prism. The $100\ \mu\text{m}$ diameter wire was held at 4.5 volts, and surrounded by a grounded cylinder of radius 3 cm.

ence fringes directly. The imaging tool allows us to detect fringes with arbitrary period (d'), and thus permitted us to study quantitatively the revivals in fringe visibility as a function of grating separation. Imaging also enabled

us to observe the fractional Talbot effect with electrons and nanostructures. The most useful result of using an imaging detector is the ability to study fringe distortions due to phase objects in the electron interferometer.

In conclusion, we demonstrated a novel electron interferometer that uses two nanostructure gratings and near-field interference effects. We demonstrated the Lau effect for electrons and observed revivals in fringe visibility when the gratings are separated by multiples of the Talbot length. This type of electron interferometer does not require spatially coherent electron waves from the electron gun, but still it tests how well the nanostructures generate and preserve coherence for electron waves. The effect of image-charge interactions between electrons and the grating structure was observed, but it does not inhibit the electron interference. The apparatus is a rudimentary sheering interferometer, and serves to demonstrate differential phase shifts. We have thus shown that metal-coated silicon nitride nanostructure gratings can be used as elements for coherent electron optics.

The authors acknowledge D. Bentley for the electron gun, and Mark Robertson-Tessi for technical assistance. This work was supported by the National Science Foundation Grant No. 0354947, and No. 0526954.

-
- [1] H. F. Talbot, *Philos. Mag.* **9**, 401 (1836).
 - [2] J. M. Cowley and A. F. Moodie, *Proc. Phys. Soc. London* **70**, 486 (1957); **70**, 497 (1957); **70**, 505 (1957); **76**, 378 (1960).
 - [3] K. Patorski, *Progress in Optics* **27**, 3 (1989).
 - [4] E. Lau, *Ann. Phys.* **6**, 417 (1948).
 - [5] J. Jahns and A. W. Lohmann, *Opt. Comm.* **28**, 263 (1979); H. O. Bartelt and J. Jahns, *Opt. Comm.* **30**, 268 (1979).
 - [6] D. E. Silva, *Applied Optics* **11**, 2613 (1972).
 - [7] M. S. Chapman, C. R. Ekstrom, T. D. Hammond, J. Schmiedmayer, B. E. Tannian, S. Wehinger, and D. E. Pritchard, *Phys. Rev. A* **51**, R14 (1995).
 - [8] S. Nowak, C. Kurtsiefer, T. Pfau, and C. David, *Opt. Lett.* **22**, 1430 (1997).
 - [9] J. F. Clauser and S. Li, *Phys. Rev. A* **49**, R2213 (1994).
 - [10] B. Brezger, L. Hackermuller, S. Uttenthaler, J. Petschinka, M. Arndt, and A. Zeilinger, *Phys. Rev. Lett.* **88**, 479 (2002).
 - [11] B. Brezger, M. Arndt, and A. Zeilinger, *Journal of Optics B* **5**, S82 (2003).
 - [12] C. David, *et al.*, *App. Phys. Lett.* **81**, 3287 (2002); A. Momose, *et al.*, *Jap. J. App. Phys.* **42**, L866 (2003); A. Momose, *Jap. J. App. Phys.* **44**, 6355 (2005); T. Weitkamp, *et al.*, *App. Phys. Lett.* **86** (2005).
 - [13] A. Tonomura, *Rev. Mod. Phys.* **59**, 639 (1987).
 - [14] A. Tonomura, L. F. Allard, G. Pozzi, D. C. Joy, and Y. A. Ono, eds., *Proceedings of the International Workshop on Electron Holography* (Elsevier, 1995).
 - [15] A. Tonomura, *Electron Holography* (Springer, 1999).
 - [16] For this calculation we assumed high energy (100 keV) electrons with a de Broglie wavelength of $\lambda = 3.9\ \text{pm}$. Lower energy electrons make the Talbot length even shorter.
 - [17] T. A. Savas, S. N. Shah, M. L. Schattenburg, J. M. Carter, and H. I. Smith, *J. Vac. Sci. Technol. B* **13**, 2732 (1995); T. A. Savas, M. L. Schattenburg, J. M. Carter, and H. I. Smith, *J. Vac. Sci. Technol. B* **14**, 4167 (1996).
 - [18] G. Gronniger, B. Barwick, H. Batelaan, T. Savas, D. Pritchard, and A. Cronin, *App. Phys. Lett.* **87** (2005).
 - [19] B. McMorran, J. D. Perreault, T. A. Savas, and A. Cronin, *Ultramicroscopy* **106**, 356 (2006).
 - [20] D. W. Keith, C. R. Ekstrom, Q. A. Turchette, and D. E. Pritchard, *Phys. Rev. Lett.* **66**, 2693 (1991).
 - [21] O. Carnal and J. Mlynek, *Phys. Rev. Lett.* **66**, 2689 (1991).
 - [22] R. E. Grisenti, W. Schollkopf, J. P. Toennies, C. C. Hegerfeldt, and T. Kohler, *Phys. Rev. Lett.* **83**, 1755 (1999).
 - [23] J. D. Perreault, A. D. Cronin, and T. A. Savas, *Phys. Rev. A* **71**, 053612 (2005).